THE JOURNAL OF PHYSICAL CHEMISTRY C

Article

pubs.acs.org/JPCC

Probing the Influence of Disorder on Lanthanide Luminescence Using Eu-Doped $LaPO_4$ Nanoparticles

Jacobine J. H. A. van Hest,[†,‡] Gerhard A. Blab,[‡] Hans C. Gerritsen,[‡] Celso de Mello Donega,[†] and Andries Meijerink*[,†]

[†]Condensed Matter and Interfaces, Debye Institute for Nanomaterials Science, Utrecht University, Princetonplein 5, 3584 CC Utrecht, The Netherlands

[‡]Molecular Biophysics, Utrecht University, Princetonplein 5, 3584 CC Utrecht, The Netherlands

ABSTRACT: Lanthanide-doped nanocrystals (NCs) differ from their bulk counterparts due to their large surface to volume ratio. It is generally assumed that the optical properties are not affected by size effects as electronic transitions occur within the well-shielded 4f shell of the lanthanide dopant ions. However, defects and disorder in the surface layer can affect the luminescence properties. Trivalent europium is a suitable ion to investigate the subtle influence of the surface, because of its characteristic luminescence and high sensitivity to the local environment. Here, we investigate the influence of disorder in NCs on the optical properties of lanthanide dopants by studying the inhomogeneous linewidth, emission intensity ratios, and luminescence decay curves for $LaPO_4$:Eu^{3+} samples of different sizes (4 nm to bulk) and core−shell configurations (core, core−isocrystalline shell, and core−silica shell). We show that the emission linewidths increase strongly for NCs. The ratio of the intensities of the forced electric dipole (ED) and magnetic dipole (MD) transitions, a measure for the local symmetry distortion around Eu^{3+} ions, is higher for samples with a large fraction of Eu^{3+} ions close to the surface. Finally, we present luminescence decay curves revealing an increased nonradiative decay rate for Eu^{3+} in NCs. The effects are strongest in core and core−silica shell NCs and can be reduced by growth of an isocrystalline $LaPO_4$ shell. The present systematic study provides quantitative insight into the role of surface disorder on the optical properties of lanthanide-doped NCs. These insights are important in emerging applications of lanthanide-doped nanocrystals.

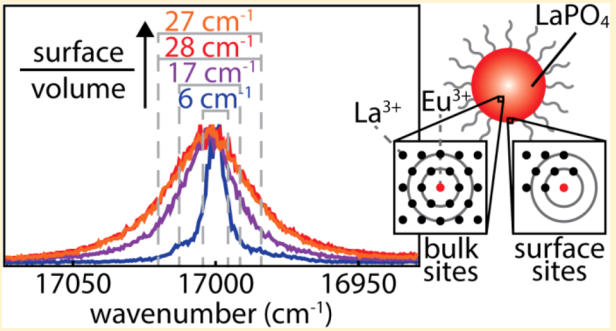

INTRODUCTION

Lanthanide-doped nanocrystals (NCs) have attracted much research interest in previous decades due to their efficient and characteristic luminescence properties which enable applications in, e.g., bioimaging,[1] nanothermometry,[2] and luminescent solar concentrators.[3] These NCs differ from their bulk counterparts in their large surface to volume ratio. As a result, a larger fraction of atoms is positioned at the surface where defects and disorder are present. It is commonly assumed that this does not affect the optical properties which are expected to be the same for lanthanide ions in NCs as in bulk material. The shielding of the 4f orbitals by filled outer 5s and 5p orbitals prevents an influence of the local surroundings on the inner $4f^n$ transitions of lanthanides. In addition, the local coordination of the lanthanide ion is the same for nanocrystalline and bulk crystalline material with the same crystal structure.[3,4] However, a subtle but important influence of the nanosize is possible.

The influence of surface ions on the luminescence properties has been studied previously. Inhomogeneous broadening of excitation and emission lines,[5−7] new sites,[8−10] and different crystal phases[7] have been observed for different lanthanide-doped inorganic NCs. In addition, the luminescence lifetime has been shown to be affected in NCs and explained by an increase in nonradiative decay through multiphonon relaxation induced by high energy vibrations of surface ligands.[11,12] A systematic study of the role of size effects on the optical properties of lanthanide-doped core and core−shell NCs is, however, lacking, and it is the aim of this study to provide detailed insight into how size effects influence various optical properties of intraconfigurational $4f^n$ transitions of lanthanide ions in NCs. To this end, small (4 nm) $LaPO_4$ NCs doped with Eu^{3+} are investigated. $LaPO_4$ NCs are among the smallest Ln-doped NCs that can be made with a narrow size distribution. The small 4 nm size gives rise to a large surface to volume ratio. In addition, the influence of the growth of an isocrystalline $LaPO_4$ shell as well as a SiO_2 shell on the optical properties is studied, and all optical properties are compared with those of Eu^{3+} in bulk (microcrystalline) $LaPO_4$.

Europium is often used as luminescent probe.[5−11] Europium is a suitable ion to investigate the influence of (surface) disorder on the luminescence properties of NCs due to its characteristic luminescence and high sensitivity to changes in

Received: July 4, 2017
Revised: August 11, 2017
Published: August 11, 2017

DOI: 10.1021/acs.jpcc.7b06549
J. Phys. Chem. C 2017, 121, 19373−19382

the local environment. $LaPO_4$ is a good host material, since europium in $LaPO_4$ shows bright luminescence and the synthesis methods are well-known for both crystalline bulk and nanomaterials.[13,14]

Several groups have studied the luminescence properties of $LaPO_4:Eu^{3+}$, bulk and nanocrystalline, in the past. Europium in $LaPO_4$ substitutes on the La^{3+} site with C_1 site symmetry.[13] The low symmetry lifts the degeneracy of the $^{2S+1}L_J$ states completely.[15] Dexpert-Ghys et al.[13] have identified 3 different europium sites in $LaPO_4:Eu^{3+}$ (2%) bulk material by performing high resolution luminescence measurements at 77 K. Disorder in the NC surface layer can give rise to new Eu^{3+} surface sites and increased inhomogeneous broadening. These surface-related effects are expected to be reduced by growth of an isocrystalline (undoped) $LaPO_4$ shell around the NCs, and this has been demonstrated by site-selective spectroscopy measurements at 30 K.[14] A later study has revealed that emission spectra of $LaPO_4:Eu^{3+}$ NCs recorded at 15 K show narrower emission lines for NCs annealed at 1000 °C than for the as-synthesized NCs. This has been explained by particle growth at 1000 °C which reduces the surface to volume ratio of the NCs.[16] Moreover, Yu et al. have demonstrated that changing the shape of the material results in extra sites in the material by performing high resolution luminescence measurements on microparticles, microrods, nanowires, and nanoparticles at 10 K.[17] Finally, Ruan et al. have identified surface states in $TbPO_4:Eu^{3+}$ NCs by measuring excitation spectra of $TbPO_4:Eu^{3+}$ bulk and NC samples at room temperature.[18]

In none of the studies mentioned above the emission linewidths of bulk and NCs have been measured and compared with each other, and also the role of shell growth has not been systematically investigated. In addition, measurements have not been performed at 4 K which is needed to reduce thermal line broadening. Moreover, the intensity ratios of the forced electric dipole (ED) and magnetic dipole (MD) transitions have not been compared, and decay curves have not been shown or measured in most studies. As a result, no comprehensive systematic study on the role of surface and disorder effects in nanocrystallline materials has been reported for the optical properties of lanthanide ions in NCs. Here, we provide a detailed comparison between the optical properties for $LaPO_4:Eu^{3+}$ bulk, core NCs, and core−shell NCs with a pure (undoped) $LaPO_4$ or silica shell.

In this work, the role of disorder and surface effects on the optical properties is investigated through analysis of the emission linewidth, ratios of the emission intensities, and luminescence decay curves for $LaPO_4:Eu^{3+}$ (2%) samples of different sizes and core−shell compositions. High resolution spectra of micro-, and nanocrystalline $LaPO_4:Eu^{3+}$ are measured at 4 K and show a significant increase in emission linewidth for Eu^{3+} in the NCs. Core−shell NCs with a $LaPO_4$ shell around the core have narrower linewidths while a silica shell does not result in narrower lines. The ratio of the ED to MD transition intensities is measured, and the lowest ED/MD ratio is observed for bulk material, followed by $LaPO_4:Eu^{3+}$/$LaPO_4$ core−shell NCs, and $LaPO_4:Eu^{3+}$-silica and $LaPO_4:Eu^{3+}$ core NCs. Finally, we present decay curves of the Eu^{3+} emission in all samples. The bulk sample shows monoexponential decay, while multiexponential decays are observed for the various NCs. Growth of an isocrystalline $LaPO_4$ shell around the core NCs results in longer decay times and a higher quantum yield while the growth of a silica shell does not affect the lifetime and the quantum yield of the nanoparticles. The results provide quantitative insight and understanding into how size effects influence the optical properties of lanthanide ions in NCs and how isocrystalline shell growth can reduce these effects.

EXPERIMENTAL SECTION

Chemicals. The chemicals used in the various synthesis procedures were La_2O_3 (Merck), Eu_2O_3 (Highways International, 4N), diammonium phosphate (Merck, 99%), $LaCl_3 \cdot 6H_2O$ (Strem chemicals, 99.9%), $EuCl_3 \cdot 6H_2O$ (Fisher Scientific, 99.9%), tributyl phosphate (Fluka Analytical, ≥ 99%), diphenyl ether (Sigma-Aldrich, 99%), tributylamine (Sigma-Aldrich, ≥99%), phosphoric acid (Aldrich, ≥99.9%), dihexyl ether (Aldrich, 97%), dodecylamine (Acros Organics, 98%), poly(5)oxyethylene-4-nonylphenyl-ether (Igepal Co 520, Sigma-Aldrich), tetraethyl orthosilicate (TEOS, Sigma-Aldrich, 99%), and ammonia 28% in water stored at 7 °C (Sigma-Aldrich, 99.9%), methanol (Sigma-Aldrich, 99.8%), cyclohexane (Sigma-Aldrich, anhydrous, 99.5%), ethanol (Alfa Aesar, 96%), and toluene (Sigma-Aldrich, anhydrous, 99.8%). All chemicals were used as received.

Synthesis of $LaPO_4:Eu^{3+}$ (2%) Bulk. Microcrystalline $LaPO_4$ doped with 2% europium was synthesized using the method described by Dexpert-Ghys et al.[13] Stoichiometric amounts of lanthanide oxide (98% La_2O_3 and 2% Eu_2O_3) and diammonium phosphate were mixed, ground in an agate mortar, and subsequently fired at 800 °C for 1 h. The mixture was ground again and fired for a second time at 1100 °C for 12 h.

Synthesis of $LaPO_4:Eu^{3+}$ (2%) Core NCs. $LaPO_4$ nanocrystals (NCs) doped with 2% europium were synthesized using a method pioneered by Haase and co-workers.[14] A clear solution of 10 mmol lanthanide chlorides (9.98 mmol lanthanum chloride and 0.02 mmol europium chloride) in 10 mL methanol was mixed with 40 mmol tributyl phosphate. Subsequently, methanol was removed under vacuum at room temperature in a Schlenk line. Next, 30 mL diphenyl ether was added and water released by the hydrated salts was removed under vacuum at 105 °C. The system was purged with nitrogen in a Schlenk line, and the temperature was allowed to drop. At temperatures below 50 °C, 40 mmol of tributylamine was added, followed by 7 mL of a 2 M solution of phosphoric acid in dihexyl ether. The reaction mixture was kept overnight (~16 h) under a nitrogen atmosphere at 200 °C to allow for particle growth. After cooling, the NCs were precipitated from the reaction mixture by addition of toluene, washed with methanol and toluene, and dried under vacuum. The NCs could be redispersed in polar media.

Synthesis of $LaPO_4:Eu^{3+}$ (2%)/$LaPO_4$ Core−Shell NCs. For the synthesis of core−shell NCs,[14,19] 7.0 mL of a 2 M solution of phosphoric acid in dihexyl ether was added to half of the crude reaction mixture (no isolation and purification of core NCs). The reaction mixture was then stirred vigorously and heated to 200 °C. Separately, a solution of 10 mmol lanthanum chloride in 10 mL of methanol was mixed with 40 mmol tributyl phosphate. After the methanol and water had been removed from the solution by heating to 105 °C under vacuum, the solution was mixed with 40 mmol tributylamine and subsequently added to the reaction mixture (2.5 mL every 5 min). The reaction mixture was then kept at 200 °C under a nitrogen atmosphere overnight (~16 h) to allow for particle growth to the final size and annealing of the NCs. The core−shell NCs were isolated from the reaction mixture using the same method as for the core NCs.

DOI: 10.1021/acs.jpcc.7b06549
J. Phys. Chem. C 2017, 121, 19373−19382

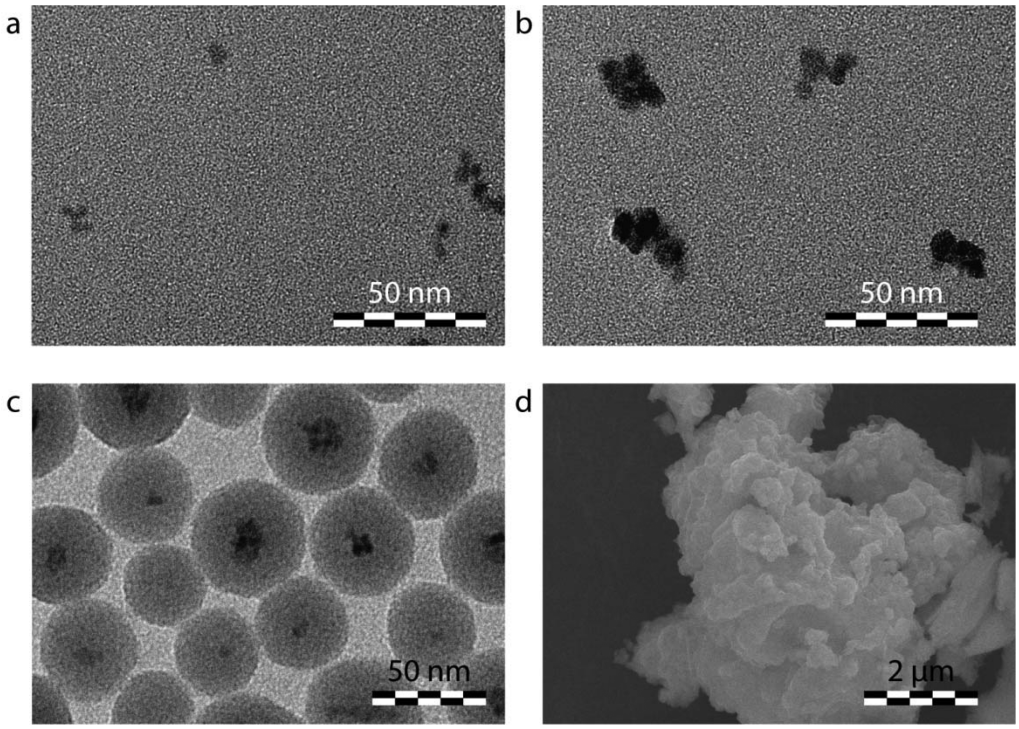

Figure 1. TEM images of the nanomaterials (A–C): (A) $LaPO_4$:Eu^{3+} core NCs, (B) $LaPO_4$:Eu^{3+}/$LaPO_4$ core–shell NCs, (C) $LaPO_4$:Eu^{3+} NCs coated with silica. (D) SEM image of the bulk material.

Ligand Exchange. We can vary the medium in which the NCs can be suspended from polar to apolar by changing the ligand attached to the surface of the NC. A ligand exchange reaction was performed in order to change the short tributylamine ligand with the longer dodecylamine ligand. Recapping of the NCs was performed by adding the dry NCs to dodecylamine heated at 200 °C. After 10 min, the heating was stopped, and the NCs were precipitated from the reaction mixture by addition of methanol followed by centrifugation. The NCs were washed several times with toluene and methanol and dried under vacuum. The NCs could be dispersed in apolar solvents after this recapping procedure.

Silica Coating of $LaPO_4$:Eu^{3+} (2%) Core NCs. Silica shells were grown around the $LaPO_4$:Eu^{3+} (2%) NCs using the inverse micelle method described previously.[20,21] First, 13 mL of Igepal Co 520 (NP-5) was dispersed in 100 mL cyclohexane and stirred at 850 rpm for 15 min. Next, 15 mg dodecylamine-capped $LaPO_4$ NCs in 10 mL of cyclohexane was injected. Subsequently, 800 μL tetraethyl orthosilicate (TEOS) and 1.50 mL of ammonia were added. The reaction mixture was stirred at 850 rpm for 15 min between every addition and for 1 min after the last addition and stored in a dark room for 1 day. The silica-coated $LaPO_4$ NCs were isolated from the reaction mixture by addition of 30 mL ethanol and centrifugation at 3000 rpm for 10 min. The sediment was redispersed in 100 mL ethanol and centrifuged at 3000 rpm for 20 min. This last step was repeated, but with centrifugation for 40 min after which one-quarter of the silica-coated $LaPO_4$ NCs was redispersed in 25 mL ethanol and the other three-quarters were dried under vacuum to obtain a white powder.

XRD. X-ray diffraction patterns of powder samples were recorded with a PW1729 Philips diffractometer equipped with a Cu Kα X-ray source (λ = 1.5418 Å). Reference diffractograms were taken from the International Center of Diffraction Data (ICDD).

TEM. The purified NCs and silica samples were characterized with transmission electron microscopy (TEM). Samples for analysis were obtained by dissolving 0.5 mg of NCs in 3 mL of ethanol and dropcasting the NC solutions on coated copper TEM grids. The TEM images were obtained with a Tecnai 12 microscope operating at 120 kV equipped with a tungsten filament. Images were recorded with a SIS CCD camera Megaview II in iTEM software.

SEM. The bulk sample was characterized with scanning electron microscopy (SEM). The sample for analysis was obtained by placing a thin layer of sample on an SEM stub with carbon tape. A 4 nm layer of platina was sputtered on top of the sample. SEM images were obtained with a XL30S FEG microscope operating at 20 kV. Images were recorded in Scandium software.

Luminescence Measurements. High resolution emission spectra of powders were recorded using an Ekspla NT342B tunable laser set at 250 nm (repetition rate 10 Hz, pulse width 6 ns) for excitation of Eu^{3+} ions in the charge transfer (CT) band. The emitted light was dispersed with a Triax 550 single emission monochromator (Jobin Yvon, 1200 line grating blazed at 400 nm) and detected with a Hamamatsu R928 detector and a Stanford Research SR400 gated photon counter set with a gate of 40 ms. Timing was controlled with a Stanford Research DG535 pulse generator. The spectral bandwidth of the monochromator was 0.06 nm (1–2 cm^{-1}). The samples were cooled to 4 K in an Oxford Instruments liquid helium flow cryostat.

Emission spectra of bulk powder and NC dispersions were recorded at room temperature using an Edinburgh Instruments FLS920 fluorescence spectrometer. Emission spectra were recorded using a 450 W Xe lamp as excitation source and a Hamamatsu R928 PMT detector.

Luminescence decay curves were recorded using pulsed excitation from an optical parametric oscillator (OPO) system

DOI: 10.1021/acs.jpcc.7b06549
J. Phys. Chem. C 2017, 121, 19373–19382

(Opotek HE 355 II) pumped by the third harmonic of a Nd:YAG laser. The OPO was tuned to λ_{exc} = 465 nm to excite the Eu^{3+} $^7F_0 \rightarrow {}^5D_2$ f–f transition (repetition rate 10 Hz, pulse width 10 ns). Decay curves were recorded by detecting the $^5D_0 \rightarrow {}^7F_1$ emission band with a Hamamatsu H7422-40 photomultiplier tube in combination with time-correlated single-photon counting (TCSPC, Edinburgh TCC900).

RESULTS AND DISCUSSION

$LaPO_4$:Eu^{3+} bulk, $LaPO_4$:Eu^{3+} core nanocrystals (NCs), $LaPO_4$:Eu^{3+}/$LaPO_4$ core–shell NCs, and $LaPO_4$:Eu^{3+} core NCs with a silica shell, all with a dopant concentration of 2%, were synthesized by methods described previously in the literature.[13,14,20,21] The size of the crystallites in the different samples is important, since it determines the fraction of (dopant) atoms at the surface which can affect the luminescence properties. The size and shape of the different samples were studied with electron microscopy. In Figure 1, transmission electron microscope (TEM) images of nanoparticles and a scanning electron microscope (SEM) image of bulk crystals are shown. The $LaPO_4$:Eu^{3+} core NCs have a size of 3.9 ± 0.7 nm as can be seen in Figure 1a. Two types of core–shell systems were investigated: an isocrystalline (undoped) $LaPO_4$ or silica shell were grown around a fraction of the core NCs. After the growth of a $LaPO_4$ shell around the core NCs, the size increases to 6.5 ± 1.3 nm, as shown in Figure 1b. This indicates that the shell growth was successful. The $LaPO_4$ NCs coated with a silica layer are shown in Figure 1c. Spherical silica particles with a size of 43 ± 4.7 nm are obtained. The $LaPO_4$ NCs are located in the center of the sphere. Many of the silica spheres contain only a single NC. However, silica spheres with no or multiple NCs are observed as well. The SEM image of the bulk material is shown in Figure 1d. A microsized structure is observed with larger crystalline domains than the nanomaterials.

The crystal structure of both bulk and nanomaterials is an important parameter for understanding the luminescence properties. $LaPO_4$ crystallizes in the monoclinic monazite structure under ambient conditions. X-ray diffractograms (XRDs) were recorded to investigate the structure of microcrystalline (bulk) $LaPO_4$:Eu^{3+}, $LaPO_4$:Eu^{3+} core NCs, $LaPO_4$:Eu^{3+}/$LaPO_4$ core–shell NCs, and $LaPO_4$:Eu^{3+} core NCs coated with silica (Figure 2). A monazite reference diffractogram is included in the same figure. The bulk material, the core NCs, and the cores with a $LaPO_4$ shell show diffraction peaks that are consistent with the monazite structure for $LaPO_4$. The narrow diffraction peaks for the bulk material are consistent with the presence of microcrystals. In contrast, the observation of broad diffraction peaks for the core and core–shell NC samples indicates the formation of nanosized particles. In addition, the diffraction peaks for the core NCs are broader than those of the core–shell NCs, which demonstrates that the core–shell NCs are characterized by larger crystalline domains than the core NCs. This shows that the $LaPO_4$ shell growth was successful and that an isocrystalline shell is grown around the nanocrystalline cores. The mean sizes of the particles can be estimated by using the Debye–Scherrer method.[22,23] Analysis using the Debye–Scherrer method yields a diameter of approximately 3.9 nm for the core NCs and of approximately 5.9 nm for the core–shell NCs. These sizes agree well with the sizes obtained with TEM. In contrast to the XRD patterns of the bulk, core, and core–shell $LaPO_4$ NCs, the XRD of the silica-coated NCs does not reproduce the monazite reference diffractogram. For these particles, the XRD is dominated by a broad band around 20° which is characteristic for amorphous silica.[24] However, around 2θ = 30° and 42° small diffraction peaks can be observed, consistent with the position of the strongest diffraction peaks of the $LaPO_4$ monazite phase.

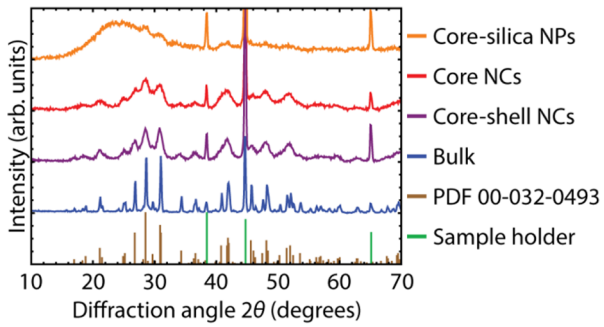

Figure 2. XRD patterns of various $LaPO_4$ materials: bulk (microcrystalline) $LaPO_4$:Eu^{3+} (blue line); $LaPO_4$:Eu^{3+}/$LaPO_4$ core-shell NCs (purple line); $LaPO_4$:Eu^{3+} core NCs (red line); $LaPO_4$:Eu^{3+} NCs coated with silica (orange line). Reference patterns of the monazite structure (PDF 00-032-0493) and sample holder are indicated in brown and green, respectively.

Spectral Width Emission Lines. High resolution emission spectra were recorded at 4 K to investigate the role of disorder and surface effects on the luminescence spectra of the various samples. Two effects were investigated: the spectral width of emission lines and the ratio of intensities between magnetic dipole (MD) and forced electric dipole (ED) transitions. The spectral resolution of the monochromator is important in these experiments as this can affect the measured linewidths. A bandpass of 0.06 nm (1–2 cm^{-1}) was used as the spectral width of the lines was typically larger than 1–2 cm^{-1}. In addition, the measurements were performed at 4 K to reduce thermal line broadening, and the measured linewidths reflect the inhomogeneous broadening. Figure 3a shows the emission spectra (λ_{exc} = 250 nm) of $LaPO_4$:Eu^{3+} bulk (blue line), $LaPO_4$:Eu^{3+}/$LaPO_4$ core–shell NCs (purple line), $LaPO_4$:Eu^{3+} core NCs (red line), and $LaPO_4$:Eu^{3+} core NCs coated with silica (orange line). All emission spectra show several sharp emission lines at similar energies, indicating that Eu^{3+} occupies the same main crystallographic site in all samples. The emission lines, resulting from intraconfigurational $4f^6$ transitions, are assigned to $^5D_0$–$^7F_1$ (588–600 nm) and $^5D_0$–$^7F_2$ (610–625 nm) transitions. The $^5D_0$–$^7F_1$ and $^5D_0$–$^7F_2$ emissions give rise to multiple emission lines, originating from transitions of the $^5D_0$ level to different crystal field levels of the $^7F_1$ and $^7F_2$ states. The ^7F_J levels, with J = 1, 2, 3, 4, 5 and 6, can be split up in a maximum of $2J$ + 1 sublevels by the crystal field induced by ligands surrounding Eu^{3+}. The degeneracy of the ^7F_J levels is completely lifted for Eu^{3+} in $LaPO_4$ with C_1 symmetry.[13,15] Part of the energy level diagram of Eu^{3+} in C_1 symmetry is schematically shown in Figure 3c. In this figure, the individual crystal field sublevels are only shown for the $^7F_1$ and $^7F_2$ levels. The origin of transitions of europium ions in microcrystalline $LaPO_4$ has been studied in detail by Dexpert-Ghys et al.[13] In their study, three different Eu^{3+} sites have been identified for bulk $LaPO_4$:Eu^{3+}. However, the emission mainly originates from one main site. The spectral positions observed for the Eu^{3+} emission lines in the present work are in good agreement with the results in ref 13. The presence of multiple sites is observed in the emission spectrum of bulk $LaPO_4$:Eu^{3+}

DOI: 10.1021/acs.jpcc.7b06549
J. Phys. Chem. C 2017, 121, 19373–19382

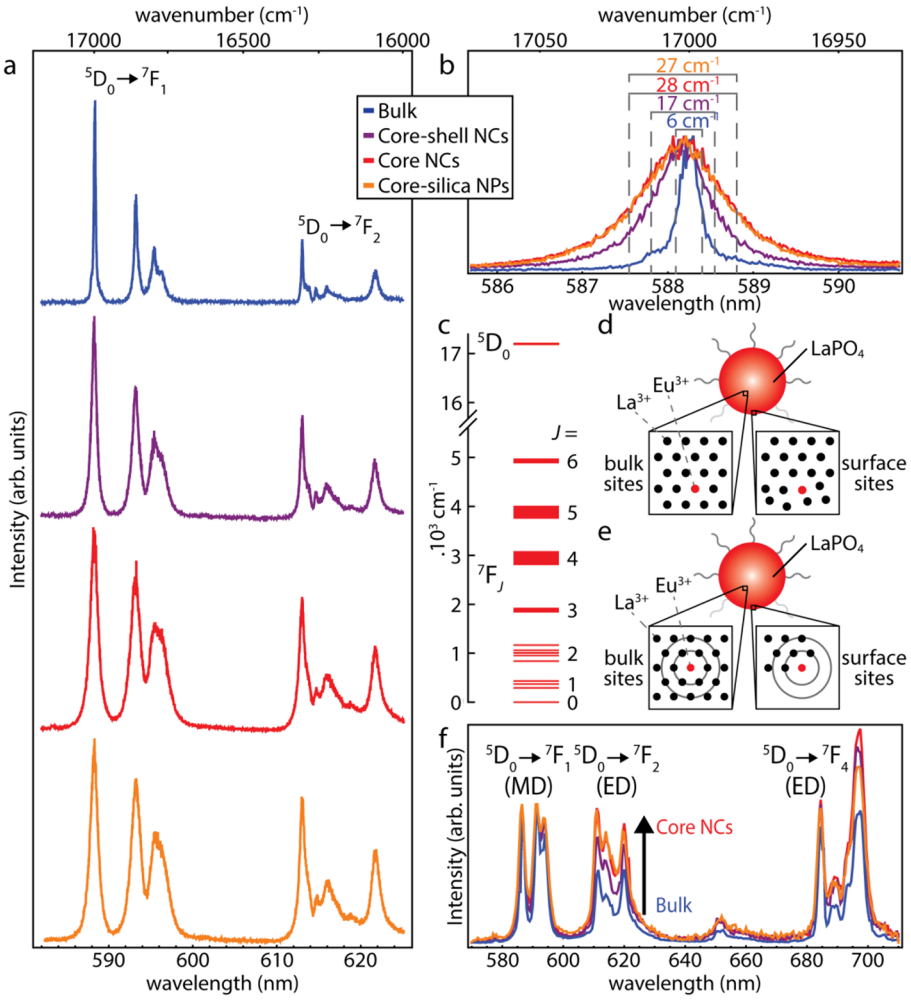

Figure 3. (A) High resolution emission spectra (λ_{exc} = 250 nm) recorded at 4 K of $LaPO_4:Eu^{3+}$ bulk (blue line), $LaPO_4:Eu^{3+}/LaPO_4$ core−shell NCs (purple line), $LaPO_4:Eu^{3+}$ core NCs (red line), and $LaPO_4:Eu^{3+}$ core−silica NPs (orange). (B) Zoom of emission spectra shown in part A. (C) Part of the energy level diagram of a Eu^{3+} ion in C_1 symmetry. The individual crystal field sublevels are only shown for the $^7F_1$ and $^7F_2$ levels. (D, E) Schematic representation of europium ions inside (bulk sites) and at the surface (surface sites) in a NC. Eu^{3+} ions at bulk sites have a highly ordered environment, while Eu^{3+} ions at surface sites have (D) an altered bond length with their neighbors or (E) miss a fraction of their neighbors. Note that for clarity only the cations are shown. (F) Emission spectra (λ_{exc} = 250 nm) of $LaPO_4:Eu^{3+}$ bulk and NCs suspended in ethanol at room temperature: $LaPO_4:Eu^{3+}$ bulk (blue line); $LaPO_4:Eu^{3+}/LaPO_4$ core−shell NCs (purple line); $LaPO_4:Eu^{3+}$ core NCs (red line); $LaPO_4:Eu^{3+}$ core NCs coated with silica (orange line).

recorded at 4 K shown by the blue line in Figure 3b. The weak feature around 587.8 nm originates from a different Eu^{3+} site.

The widths of the emission lines were determined for the various samples and compared with each other. A zoom in of the emission line for transition from the $^5D_0$ level to the lowest crystal field level of the $^7F_1$ state, which is approximately at 588 nm (17000 cm^{-1}), is shown in Figure 3b for the various samples. The full width at half-maximum (fwhm) was determined by fitting the data with Gaussian functions and is indicated in the figure and listed in Table 1. The bulk sample shows the narrowest emission lines with a typical fwhm of 6 cm^{-1}. In contrast, the core NCs show broader emission lines and have the largest fwhm, 28 cm^{-1}.

The broadening of the emission lines for NCs can be explained by the difference in environment for Eu^{3+} ions at the surface compared with Eu^{3+} ions inside the NC. Two models can describe this difference in environment, schematically shown in Figure 3d,e. Note that for clarity only the cations are shown. First, ions at the surface can have an altered bond length after surface reconstruction, leading to an increased degree of disorder compared with ions inside the crystal. A schematic representation of this situation is shown in Figure 3d. Second, for ions at the surface of the NC the periodic crystal structure

Table 1. Overview of Parameters of Luminescence Properties for the $LaPO_4:Eu^{3+}$ Bulk, $LaPO_4:Eu^{3+}/LaPO_4$ Core−Shell NCs (NCs), $LaPO_4:Eu^{3+}$ Core NCs, and $LaPO_4:Eu^{3+}$ Core−Silica Nanoparticles (NPs)[a]

sample	fwhm (cm^{-1})	measured R	τ_1 (ms)	τ_2 (ms)
bulk	6	0.81 (0.97)	3.1	
core−shell NCs	17	1.03	1.9	4.7
core NCs	28	1.24	1.6	3.8
core−silica NPs	27	1.20	1.4	3.8

[a]Parameters include the inhomogeneous linewidth (full width at half maximum) of the $^5D_0$−$^7F_1$ emission line at 588 nm, the ratio R of intensities of the $^5D_0$−$^7F_1$ magnetic dipole transition and the $^5D_0$−$^7F_2$ forced electric dipole transition (the ratio between brackets is after correction for refractive index effects, see text), and the luminescence lifetimes obtained from fits to a single exponential (bulk) or biexponential (NCs) decay.

DOI: 10.1021/acs.jpcc.7b06549
J. Phys. Chem. C 2017, 121, 19373−19382

ends, and as a result, the surface ions miss a fraction of their second neighbors and perhaps third and fourth neighbors. This situation is sketched in Figure 3e. The crystal field the europium ions experience is determined by the local structure around the ion.[25] In both models, the local structure around europium ions at the surface is different from that for europium ions inside the NC, resulting in variations in the crystal field. Consequently, the positions of the energy levels of surface europium ions vary slightly compared with those of ions in the interior of the NC. As a result, broader emission lines are obtained for NCs with a large fraction of (europium) atoms positioned at the surface.

Core−shell NCs with an isocrystalline $LaPO_4$ shell around the core show narrower peaks than the core NCs. However, the peaks are broader than those in the bulk material. A fwhm of 17 cm^{-1} is obtained for the transition around 588 nm. After growth of an isocrystalline undoped $LaPO_4$ shell around the $LaPO_4$:Eu^{3+} core NCs, Eu^{3+} ions initially positioned close to the surface are now more in the interior of the NCs. As a result, the local environment and the crystal field around these ions more closely resemble the coordination of ions inside the NC. Consequently, the decrease in disorder around the Eu^{3+} ions reduces variation in the positions of the energy levels, and narrower emission lines are obtained. However, the environment around these ions is clearly not the same as for europium ions in bulk material, since the emission lines are broader than in bulk. The silica-coated core NCs show the same linewidths as the core NCs and have a fwhm of 27 cm^{-1}. This indicates that the disorder at the $LaPO_4$ surface is similar to those of the core NCs. This is not unexpected. The silica coating has a different structure than $LaPO_4$, and after silica coating, the surface atoms in the coated $LaPO_4$ NCs are still situated at a disrupted interface. The similarity in spectral width before and after silica coating indicates that the influence of disorder on the linewidth does not depend on the type of surface termination (surface atoms coordinated by a layer of ligands or silica). The increase in spectral linewidth is substantial: from 6 to 28 cm^{-1}. The observation of such a large inhomogeneous linewidth in the NCs is explained by the small size (~4 nm) of the NCs. For larger NCs, narrower lines are expected as the role of surface disorder will decrease with a smaller surface to volume ratio. It will be interesting to monitor the linewidth as a function of particle size and also to measure the inhomogeneous linewidth for different types of Eu^{3+}-doped NCs of the same size to study differences in inhomogeneous broadening for different NC host materials.

Intensity Branching Ratios. The various transitions in europium have different dipole characters. The $^5D_0$−$^7F_1$ transition is a magnetic dipole (MD) transition and is allowed by the Laporte selection rule, but the transition probability of MD transitions is low, typically 10^6 times smaller than that of fully allowed electric dipole (ED) transitions.[25,26] The $^5D_0$−$^7F_2$, $^7F_4$, and $^7F_6$ transitions are electric dipole transitions and are forbidden by the Laporte selection rule. However, this selection rule is relaxed by mixing of opposite parity states into the $4f^6$ states by the odd-parity crystal field components. Because of this, the transitions are known as forced electric dipole transitions. The extent of mixing is dependent on the local symmetry around the europium ion and the energetic position of opposite parity states. Mixing increases when a europium ion is placed on a site which deviates more strongly from inversion symmetry and/or for Eu^{3+} ions with low energy opposite parity states. The formal site symmetry for Eu^{3+} in $LaPO_4$ is C_1, the lowest possible symmetry. On the basis of the relatively high intensity of the $^5D_0$−$^7F_1$ MD transition around 590 nm, it is clear that the deviation from inversion symmetry is not as large as in other host lattices. Typically, forced ED and MD transitions have comparable intensities for transitions within the $4f^n$ configuration of Ln^{3+} ions with generally a higher intensity for forced ED transitions when the Ln ion is not in inversion symmetry. For Eu^{3+}, the $^5D_0$ − $^7F_2$ transition usually dominates when Eu^{3+} is not in inversion symmetry. However, for Eu^{3+} in $LaPO_4$, in spite of the formally lowest possible site symmetry (C_1), the relative intensity of the $^5D_0$ − $^7F_2$ is comparable to the $^5D_0$−$^7F_1$ MD transition which is lower than expected.

The intensity of forced ED transitions depends on the distortion of the local surroundings from inversion symmetry. The MD transition probability is largely independent of the local environment (except for refractive index effects, vide infra). This implies that a distortion of the local symmetry, as it occurs at the NC surface, may lead to a higher relative intensity of the forced ED transitions on Eu^{3+}. The low relative intensity of the $^5D_0$−$^7F_2$ transition for Eu^{3+} in $LaPO_4$ indicates that the odd-parity crystal field components are weak. Local distortions (surface effects and defects such as vacancies, dislocations and interstitial defects) will enhance the deviation from inversion symmetry and can thus induce an increase in the relative intensity of the forced ED transitions.[27] We will refer to this as lowering of the symmetry. Note that the formal site symmetry C_1 is the lowest possible and that lowering of the symmetry here means a stronger deviation from inversion symmetry as a result of local (surface-related) distortions. To investigate this effect, emission spectra were recorded, and the intensity ratio of the $^5D_0$−$^7F_1$ (MD) to the $^5D_0$ − $^7F_{2,4}$ (forced-ED) was analyzed. The emission spectra, corrected for the instrumental response, are shown in Figure 3f and scaled to the $^5D_0$−$^7F_1$ emission intensity. Before further discussing the results, it is important to estimate to what extent the ratio is affected by changes in the local refractive index n as the dependence of ED and MD transition rates on n is different.

The rate of the MD transition is dependent on the surrounding refractive index and can be described by[25,28]

$$k_{MD}(n) = k^0_{MD} n^3 \tag{1}$$

where $k_{MD}(n)$ is the decay rate for a magnetic dipole transition in a medium with refractive index n, k^0_{MD} the decay rate for a magnetic dipole transition in vacuum, and n the refractive index of the medium surrounding the emitter. The rate of the ED transitions can be described by the nanocavity model[19]

$$k_{ED}(n) = k^0_{ED} n \left(\frac{3n^2}{2n^2 + n^2_{NC}} \right)^2 \tag{2}$$

where $k_{ED}(n)$ is the decay rate for an electric dipole transition in a refractive index n, k^0_{ED} the decay rate for an electric dipole transition in vacuum, n the refractive index of the medium surrounding the emitter, and n_{NC} the refractive index of the NC in which the emitter is embedded.

The ratio R between the emission intensities of the ED and MD transitions can be described by dividing eq 2 by eq 1:

$$R = \frac{k_{ED}(n)}{k_{MD}(n)} = \frac{k^0_{ED}}{k^0_{MD}} \frac{1}{n^2} \left(\frac{3n^2}{2n^2 + n^2_{NC}} \right)^2 \tag{3}$$

DOI: 10.1021/acs.jpcc.7b06549
J. Phys. Chem. C 2017, 121, 19373−19382

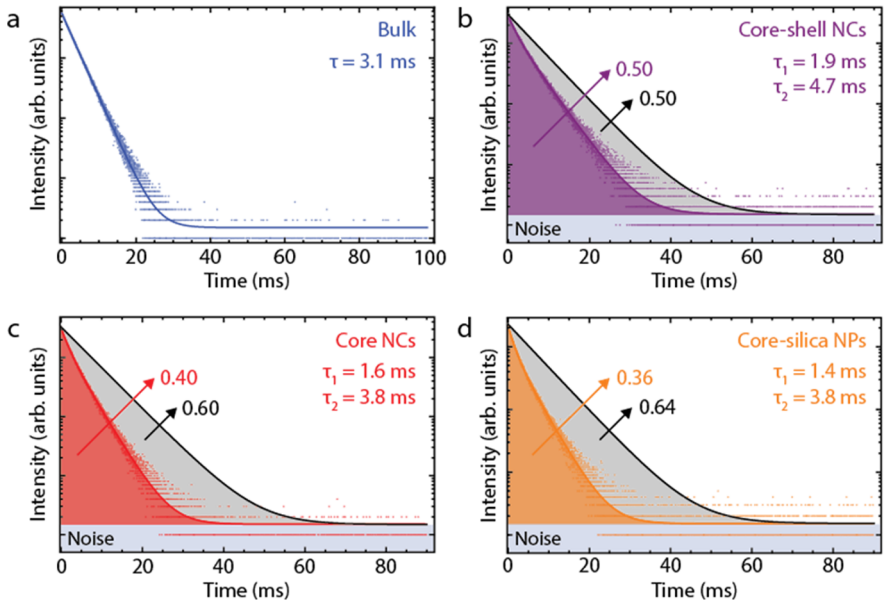

Figure 4. Luminescence decay curves of 611 nm emission for various Eu^{3+}-doped $LaPO_4$ samples excited at 465 nm (6 ns pulses). (A) $LaPO_4$:Eu^{3+} bulk, τ = 3.1 ms. (B) $LaPO_4$:Eu^{3+}/$LaPO_4$ core−shell NCs in ethanol, τ_1 = 1.9 ms, τ_2 = 4.7 ms. (C) $LaPO_4$:Eu^{3+} core NCs in ethanol, τ_1 = 1.6 ms, τ_2 = 3.8 ms. (D) $LaPO_4$:Eu^{3+} core−silica NPs in ethanol, τ_1 = 1.4 ms, τ_2 = 3.8 ms. The black lines in parts B−D are the calculated radiative decay curves with QY = 1 (Γ = 0.15 ms^{-1}, τ = 6.7 ms), and the colored and black numbers represent the fraction of radiative and nonradiative decay, respectively.

The ratio R is influenced by the refractive index of the surrounding medium as can be seen in eq 3. For this reason, it is important to know the refractive index surrounding the emitters when comparing the ratio R for the various samples in order to differentiate effects of n and the role of disorder which can change k_{ED}^0 through an increase in forced ED transition probability induced by a stronger deviation from inversion symmetry.

Emission spectra of $LaPO_4$:Eu^{3+} bulk (n = 1.79 for $LaPO_4$[29]) and NCs suspended in ethanol (n = 1.36) recorded at room temperature are shown in Figure 3f. All samples show sharp emission lines around 590 nm ($^5D_0$−$^7F_1$, MD), 610 nm ($^5D_0$−$^7F_2$, ED), and 700 nm ($^5D_0$−$^7F_4$, ED). The ratios between the $^5D_0$−$^7F_1$ and $^5D_0$−$^7F_2$ transition intensities for the various samples are listed in Table 1. We only consider the $^5D_0$−$^7F_2$ transition for the ED intensity, since this transition is most sensitive to changes in the local environment around Eu^{3+}.[15,30,31] The ratio R expected for the bulk sample when embedded in a surrounding medium with the refractive index of ethanol is calculated with eq 3 and included in the same table. The refractive index corrected ED/MD ratio obtained for bulk material is 0.97. This value is smaller than the values found for Eu^{3+} in the various NCs, indicating that Eu^{3+} ions in bulk have a higher local symmetry (experience smaller odd-parity crystal field components). The $LaPO_4$:Eu^{3+}/$LaPO_4$ core−shell NCs have only a slightly lower ratio R (1.03) than for bulk, which suggests that the Eu^{3+} ions have a local symmetry similar to that of the bulk.

The $LaPO_4$:Eu^{3+} core NCs and core−silica NPs show about 20% higher ED/MD ratios. This indicates that Eu^{3+} ions at the surface of the core NCs have a more asymmetric environment, resulting in enhanced mixing of opposite parity states into the 4f states. Consequently, a higher probability and relative intensity of the ED transition is obtained. The higher forced ED transition rates can also be seen as an increase in Judd−Ofelt parameters Ω_2, Ω_4, and/or Ω_6 for Eu^{3+} on the more asymmetric surface sites.[28] From these results, we can conclude that the symmetry distortions in surface sites not only affect the energy of intraconfigurational 4f transitions (resulting in inhomogeneous broadening), but also the admixture of opposite parity states and thus the forced ED transition probability. The effect is much stronger for the core and core−silica shell NCs than for the core−isocrystalline shell NCs. By growth of a thin isocrystalline shell, the ratio is almost the same as that for bulk $LaPO_4$. This suggests that the enhanced admixture is dominated by short-range distortions, probably mainly in the local surrounding by anions around Eu^{3+}. Note the difference with the inhomogeneous broadening which is reduced for the $LaPO_4$ core-isocrystalline shell NCs, but still much larger than in bulk $LaPO_4$:Eu^{3+}. This shows that the role of disorder on inhomogeneous broadening is a longer range effect. Further research is required to investigate if this is a general trend in Ln^{3+}-doped NCs.

Luminescence Lifetimes. Lifetime measurements provide information about the various decay pathways of europium. Again, the refractive index of the environment surrounding the emitters influences the radiative decay rate, and it is important to know the refractive index n of the surrounding medium. The bulk sample was measured as powder (n = 1.79 for $LaPO_4$[29]), and the NCs were measured in an ethanol suspension (n = 1.36). Figure 4 shows the luminescence decay curves of Eu^{3+} emission in $LaPO_4$:Eu^{3+} bulk (A), $LaPO_4$:Eu^{3+}/$LaPO_4$ core−shell NCs (B), $LaPO_4$:Eu^{3+} core NCs (C), and $LaPO_4$:Eu^{3+} core−silica NPs (D), recorded for 611 nm emission. Measurements performed at different setups showed small variations in decay curves which is generally observed. Differences in excitation power, time response of detection system, and spectral width can give rise to small differences in the decay curves measured. These do not influence the general trends of the observations described below. The bulk sample shows exponential decay for the emission, and a monoexponential fit to the data points gives a decay time of 3.1 ± 0.003 ms, see Figure 4a. Here and below error margins are given as obtained with the fitting procedure. There is a larger (~0.1 ms) variation

DOI: 10.1021/acs.jpcc.7b06549
J. Phys. Chem. C 2017, 121, 19373−19382

in the decay times if slightly different time intervals or fitting procedures are used, and this reflects the actual uncertainty in decay times. This value agrees well with the 3.18 ms in $LaPO_4:Eu^{3+}$ (2%) bulk reported previously in literature.[13] The observation of monoexponential decay indicates the presence of one (main) radiative decay pathway. The quantum yield (QY) was calculated on the basis of the decay rate using the method described by Werts et al.[32] A QY of ~85% is obtained. This calculation supports our assumption that nonradiative decay is negligible and that the QY is close to 100% for the bulk sample.

The emission decay curves for the various nanocrystalline materials show multiexponential decay. It is challenging to retrieve accurate parameters from fitting nonexponential decay curves. Slight changes in the fitting procedure lead to variations in the fit parameters. For this reason, the decay curves were fitted with various functions, i.e., mono-, bi-, and triexponential functions, over various time intervals and with various weighting factors in order to get insight into the best fitting procedure. Although the various fitting procedures resulted in different fit parameters, the same general trends were observed for parameters obtained with the same fitting procedure. Here, we present the luminescence decay curves fitted over the first 20 ms with biexponential decay functions with fixed background and included statistical weighting to obtain information on differences in the decay behavior for the emission in the three classes of NCs. This gave a reasonable agreement with experiment although one has to realize that in reality decay rates for different Eu^{3+} ions will vary, and only a large number of different decay rates describes the true situation for the emission decay of the highly inhomogeneous distribution of decay rates for Eu^{3+} ions in NCs. The luminescence decay curve of Eu^{3+} emission in the $LaPO_4$ core NCs is shown in Figure 4c by the red dots. The biexponential fit, shown by the red line, gives decay times of 1.6 ± 0.03 and 3.8 ± 0.02 ms. The two lifetimes, one short and one long, can be explained by the presence of two different sites in the NC. In our model, we distinguish between Eu^{3+} close to the surface with a short lifetime and Eu^{3+} ions inside the NC with a long lifetime. Several mechanisms can contribute to the reduction in lifetime for Eu^{3+} ions close to the surface. These include the contribution of a nonradiative decay pathway caused by multiphonon relaxation and enhanced mixing of opposite parity states into the $4f^6$ states. Multiphonon relaxation can compete with radiative decay when Eu^{3+} ions couple with four nearby N−H, C−H, and O−H vibrations (phonons) of ligand and solvent molecules with energies of ~3400, 3000, and 3500 cm^{-1}, respectively, in order to bridge the $^5D_0$−$^7F_6$ energy gap of 12000 cm^{-1} in Eu^{3+}. Multiphonon relaxation becomes faster if the gap can be bridged by a smaller number of phonons and when the distance to the vibrational oscillations decreases.[33,34] As a result, Eu^{3+} ions close to the surface will have a faster nonradiative decay rate and shorter lifetime than Eu^{3+} ions in the interior of the NC. This difference between surface and interior Eu^{3+} ions is also reflected in the time gated emission spectra. Spectra collected in the first 5 ms after pulsed excitation have a higher relative intensity for the $^5D_0$−$^7F_2$ emission, while the emission spectrum collected for the 10−40 ms time window, the $^5D_0$−$^7F_1$ emission, dominates.

Next to multiphonon relaxation, admixing of opposite parity states into the $4f^6$ states by the odd-parity crystal field components can also contribute to a faster lifetime for Eu^{3+} ions close to the surface. This mixing increases if a Eu^{3+} ion is placed at a site with lower symmetry as explained above. Consequently, the forced electric dipole (ED) transition probability and the radiative decay rate increase. As a result, Eu^{3+} ions close to the surface, which are positioned on sites with lower symmetry, have a faster radiative decay rate and shorter lifetime than Eu^{3+} ions in the inside of the NC. On the basis of the variation in ED/MD transition probability ratio (Table 1), this effect can cause small (10−20%) variations in radiative decay rates. The population of ions with a fast and slow decay can be extracted from the amplitudes of the fit. For $LaPO_4:Eu^{3+}$ core NCs, 44 ± 1% has a fast decay and 56 ± 1% has a slow decay, meaning that 44% of the emitters are positioned close to the surface, which is in agreement with the theoretical fraction of 27% given the uncertainty in the fitting procedure (vide supra).

The radiative decay time of emitters depends strongly on the refractive index of the medium surrounding the emitters. In addition, the radiative decay rate consists of contributions from both magnetic and electric dipole character, which have a different dependence on the refractive index n. The radiative decay rate of emitters in NCs with QY = 1 can be calculated by combining eqs 1 and 2 and correcting for the different intensity ratios of the MD and ED transitions, which are calculated from the spectra shown in Figure 3F:

$$\Gamma_r(n) = \left(\frac{I_{MD}}{I_{tot}}\frac{\Gamma_{bulk}}{n_{NC}^3}n^3\right) + \left(\frac{I_{ED}}{I_{tot}}\frac{\Gamma_{bulk}}{n_{NC}}n\left(\frac{3n^2}{2n^2 + n_{NC}^2}\right)^2\right) \quad (4)$$

where I_{MD} is the integrated intensity of the $^5D_0$−$^7F_1$ transition, I_{ED} the integrated intensities of the $^5D_0$−$^7F_2$ and $^5D_0$−$^7F_4$ transitions, I_{tot} the sum of I_{MD} and I_{ED}, Γ_{bulk} is 0.32 ms^{-1} (τ = 3.1 ms in bulk), n_{NC} = 1.79,[29] and n = 1.36 (ethanol). A radiative decay rate, $\Gamma_r(n)$, of 0.15 ms^{-1} (τ = 6.7 ms) is obtained, shown by the black line in Figure 4c. An estimate of the upper limit of the QY can be obtained by dividing the area under the measured decay curve (red dots) by the area under the theoretically determined decay curve by eq 4 (black line). This procedure gives an upper limit for the QY of 0.40 for the Eu^{3+} luminescence in core $LaPO_4$ NCs.

The luminescence decay curve of the $^5D_0$ emission from Eu^{3+} in $LaPO_4:Eu^{3+}/LaPO_4$ core−shell NCs is shown in Figure 4b by the purple dots. A biexponential fit (purple line) yields decay times τ_1 = 1.9 ± 0.04 ms and τ_2 = 4.7 ± 0.03 ms. For $LaPO_4:Eu^{3+}/LaPO_4$ core−shell NCs, on the basis of the amplitude of the two decay signals, 41 ± 1% has a fast decay and 59 ± 1% has a slow decay. Both lifetimes are increased after the growth of an isocrystalline $LaPO_4$ shell around the core NCs. The short decay time for the $LaPO_4:Eu^{3+}$ core NCs is ascribed to Eu^{3+} ions close to the surface. The slight increase in the short decay time, τ_1, can be explained by the decrease in the nonradiative decay rate by multiphonon relaxation and the decrease in admixing of opposite parity states into the $4f^6$ states. Multiphonon relaxation becomes slower since emitters are shielded from the surface by the isocrystalline $LaPO_4$ shell; i.e., the distance between the emitters and the high energy vibrational modes of adsorbed surface ligands increases. For this reason, coupling with C−H, N−H, and O−H vibrations is reduced, and the nonradiative decay rate becomes slower.[34,35] Moreover, mixing of opposite parity states into the $4f^6$ states by the odd-parity crystal field components decreases since emitters initially positioned at surface sites with low symmetry are after shell growth positioned at sites with higher symmetry. Consequently, the forced electric dipole (ED) transitions

DOI: 10.1021/acs.jpcc.7b06549
J. Phys. Chem. C 2017, 121, 19373−19382

become more forbidden, and the radiative decay rate becomes slower. This is also seen in Figure 3f by the decrease of the emission intensity of the $^5D_0-^7F_2$ transition after shell growth. Both mechanisms result in a longer decay time for Eu^{3+} ions positioned close to the surface, although the influence of reduced multiphonon relaxation is much higher than that of the decrease in forced ED emission rate.

The long decay time for the $LaPO_4:Eu^{3+}$ core NCs is ascribed to Eu^{3+} ions inside the NC. The increase in the long decay time, τ_2, can be explained by the decrease in nonradiative decay by multiphonon relaxation through N−H, C−H, and O−H vibrations of ligand and solvent molecules. Eu^{3+} ions inside the NC couple weaker with phonons at the surface than Eu^{3+} ions close to the surface, since the distance to the oscillations is larger, but in the presently investigated small (4 nm) NCs also Eu^{3+} ions inside the NC can couple to vibrational modes of surface molecules. This distance becomes even larger after growth of an isocrystalline $LaPO_4$ shell around the core NCs. Consequently, multiphonon relaxation becomes less effective, and the nonradiative decay rate becomes slower. As a result, the lifetime increases. An upper limit for the QY of 0.50 was obtained for the $LaPO_4:Eu^{3+}/LaPO_4$ core−shell NCs using the same method described above. The radiative decay rate, $\Gamma_r(n)$, was determined to be 0.15 ms^{-1} (τ = 6.7 ms), using the constants Γ_{bulk} = 0.32 ms^{-1} (τ = 3.1 ms in bulk), n_{NC} = 1.79,[29] and n = 1.36 (ethanol).

The luminescence decay curve of Eu^{3+} emission in $LaPO_4:Eu^{3+}$ core−silica NPs is shown in Figure 4d by the orange dots. A biexponential fit (orange line) yields decay times τ_1 = 1.4 ± 0.03 ms and τ_2 = 3.8 ± 0.02 ms. These values are approximately the same as the values obtained for the core NCs. For $LaPO_4:Eu^{3+}$−silica core−shell NPs, 53 ± 1% has a fast decay and 47 ± 1% has a slow decay. The upper limit of the QY was determined to be 0.36 using the constants, $\Gamma_r(n)$ = 0.15 ms^{-1} (τ = 6.7 ms), Γ_{bulk} = 0.32 ms^{-1} (τ = 3.1 ms in bulk), n_{NC} = 1.79,[29] and n = 1.36 (ethanol). These results indicate that growth of a silica shell around the core NCs barely affects the lifetime and QY of the Eu^{3+} emission as the decay behavior resembles that of Eu^{3+} in the core NCs. This result may seem surprising as upon silica growth the surface ligands with high energy C−H and N−H vibrations are (largely) removed.[36] However, O−H groups in the silica are present and can also quench the emission through multiphonon relaxation.

The results presented demonstrate the influence of the incorporation of Eu^{3+} ions into nanocrystalline hosts in which the ions are close to the surface. For Eu^{3+} in $LaPO_4$ NCs the luminescence properties change: the emission lines broaden, forced ED transitions are enhanced, and nonradiative decay rates increase for Eu^{3+} in NCs. The extent to which the luminescence properties change depends on the type of NC. Core−shell NCs with an isocrystalline $LaPO_4$ shell around the core have narrower linewidths while growth of a silica shell does not result in narrower lines. In addition, the ratio of the ED and MD transition intensities is lowest for bulk material, followed by $LaPO_4:Eu^{3+}/LaPO_4$ core−shell NCs and $LaPO_4:Eu^{3+}$−silica and $LaPO_4:Eu^{3+}$ core NCs. Decay measurements show monoexponential decay for Eu^{3+} emission in the bulk sample, while multiexponential decay is observed for Eu^{3+} in NCs. Growth of an isocrystalline $LaPO_4$ shell around the core NCs results in longer decay times and a higher maximum QY while the growth of a silica shell does not affect the lifetime and the QY of the nanoparticles.

CONCLUSIONS

The role of the disorder in nanocrystals (NCs) on the luminescence properties of Ln^{3+} ions was investigated systematically by measuring high resolution emission spectra of $LaPO_4:Eu^{3+}$ bulk, $LaPO_4:Eu^{3+}$ core NCs, $LaPO_4:Eu^{3+}/LaPO_4$ core−shell NCs, and $LaPO_4:Eu^{3+}$ core−silica NPs. The full width at half-maximum (fwhm) of the emission lines increases strongly from 6 cm^{-1} for bulk material to 28 cm^{-1} for europium doped $LaPO_4$ NCs. The fwhm reduces to 17 cm^{-1} after coating the core NCs with an isocrystalline $LaPO_4$ shell, while coating with silica does not affect the linewidth (fwhm = 27 cm^{-1}). The variation in emission linewidths is explained by disorder in the NC surface layer, resulting in differences in the local coordination of Eu^{3+} ions which causes variations in crystal fields and thus the exact positions of the energy levels for Eu^{3+} ions in the NCs.

The ratio between the intensity of the magnetic dipole transition (MD) and the forced electric dipole (ED) transitions provides information about the deviation from inversion symmetry around the Eu^{3+} ion. The ratio is lowest for bulk material (0.81) and increases for core−shell (1.03), core (1.24), and core−silica (1.20) NCs, indicating a significant enhancement of forced ED transitions for surface Eu^{3+} ions which is explained by a stronger deviation from inversion symmetry and therefore larger Judd−Ofelt parameters.

Luminescence lifetime measurements show a monoexponential decay with τ = 3.1 ms for Eu^{3+} emission in the bulk sample and a multiexponential decay for the NCs which can be approximated by a biexponential decay function. The lifetimes and maximum QYs decrease going from core−isocrystalline shell NCs (τ_1 = 1.9 ms, τ_2 = 4.7 ms, and QY = 0.50) to core NCs (τ_1 = 1.6 ms, τ_2 = 3.8 ms, and QY = 0.40) and core−silica NPs (τ_1 = 1.4 ms, τ_2 = 3.8 ms, and QY = 0.36). The higher decay rates and lower QYs are ascribed to stronger multiphonon relaxation in NCs where Eu^{3+} ions are in close proximity to high energy vibrations of surface ligands (core and core−isocrystalline shell NCs) or hydroxyl groups (core−silica shell NCs).

The present systematic study of the role of disorder and surface on the luminescence properties of lanthanide ions in NCs can serve to understand and predict optical properties of lanthanide-doped NCs. In a first approximation, the luminescence resembles that of the bulk materials, but the reduction in quantum efficiency, subtle change in branching ratio of the emission line intensities, and strong increase in spectral linewidth can have implications for application of luminescent NCs, e.g., in nanothermometry, upconversion NCs, bioimaging, NC lasers, and optical sensing.

AUTHOR INFORMATION

Corresponding Author

*E-mail: A.Meijerink@uu.nl. Phone: +31 30 253 2202.

ORCID

Jacobine J. H. A. van Hest: 0000-0001-9665-6220
Celso de Mello Donega: 0000-0002-4403-3627
Andries Meijerink: 0000-0003-3573-9289

Author Contributions

The manuscript was written through contributions of all authors. All authors have given approval to the final version of the manuscript.

Notes

The authors declare no competing financial interest.

DOI: 10.1021/acs.jpcc.7b06549
J. Phys. Chem. C 2017, 121, 19373−19382

■ ACKNOWLEDGMENTS

The research leading to these results has received funding from European Union's Seventh Framework Programme FP7/2007-2013/for project GUIDEnano under Grant 604387.

■ REFERENCES

(1) Bouzigues, C.; Gacoin, T.; Alexandrou, A. Biological Applications of Rare-Earth Based Nanoparticles. *ACS Nano* **2011**, *5*, 8488−8505.
(2) Dong, H.; Du, S.-R.; Zheng, X.-Y.; Lyu, G.-M.; Sun, L.-D.; Li, L.-D.; Zhang, P.-Z.; Zhang, C.; Yan, C.-H. Lanthanide Nanoparticles: From Design Toward Bioimaging and Therapy. *Chem. Rev.* **2015**, *115*, 10725−10815.
(3) Huang, X.; Han, S.; Huang, W.; Liu, X. Enhancing Solar Cell Efficiency: The Search for Luminescent Materials as Spectral Converters. *Chem. Soc. Rev.* **2013**, *42*, 173−201.
(4) Blasse, G.; Grabmaier, B. C.; *Luminescent Materials*; Springer-Verlag: New York, 1994.
(5) Williams, D. K.; Bihari, B.; Tissue, B. M.; McHale, J. M. Preparation and Fluorescence Spectroscopy of Bulk Monoclinic Eu^{3+}:Y_2O_3 and Comparison to Eu^{3+}:Y_2O_3 Nanocrystals. *J. Phys. Chem. B* **1998**, *102*, 916−920.
(6) Tissue, B. M. Synthesis and Luminescence of Lanthanide Ions in Nanoscale Insulating Hosts. *Chem. Mater.* **1998**, *10*, 2837−2845.
(7) Williams, D. K.; Yuan, H.; Tissue, B. M. Size-dependene of the Luminescence Spectra and Dynamics of Eu-Y_2O_3 Nanocrystals. *J. Lumin.* **1999**, *83*−*84*, 297−300.
(8) Qi, Z.; Shi, C.; Zhang, W.; Zhang, W.; Hu, T. Local Structure and Luminescence of Nanocrystalline Y_2O_3: Eu. *Appl. Phys. Lett.* **2002**, *81*, 2857−2859.
(9) Jia, C.-J.; Sun, L.-D.; Yan, Z.-G.; Pang, Y.-C.; Lü, S.-Z.; Yan, C.-H. Monazite and Zircon Type $LaVO_4$: Eu Nanocrystals - Synthesis, Luminescent Properties and Spectroscopic Identification of Eu^{3+} Sites. *Eur. J. Inorg. Chem.* **2010**, *2010*, 2626−2635.
(10) Wei, Z.; Sun, L.; Liao, C.; Yin, J.; Jiang, X.; Yan, C.; Lu, S. Size-dependent Chromaticity in YBO_3: Eu Nanocrystals: Correlation with Microstructure and Site Symmetry. *J. Phys. Chem. B* **2002**, *106*, 10610−10617.
(11) Zhang, Y.-X.; Lu, Y.-Q.; Huang, S.-H.; Lü, S.-Z.; Yan, C.-H.; Sun, L.-D.; Liao, C.-S. Eu^{3+} Ion as Fluorescent Probe for Detecting the Surface Effect in Nanocrystals. *Appl. Phys. Lett.* **2003**, *82*, 3511−3513.
(12) Capobianco, A.; Boyer, J. C.; Vetrone, F.; Speghini, A.; Bettinelli, M. Optical Spectroscopy and Upconversion Studies of Ho^{3+} Doped Bulk and Nanocrystalline Y_2O_3. *Chem. Mater.* **2002**, *14*, 2915−2921.
(13) Dexpert-Ghys, J.; Mauricot, R.; Faucher, M. D. Spectroscopy of Eu^{3+} Ions in Monazite Type Lanthanide Orthophosphates $LnPO_4$, Ln= La or Eu. *J. Lumin.* **1996**, *69*, 203−215.
(14) Lehmann, O.; Kömpe, K.; Haase, M. Synthesis of Eu^{3+}-doped Core and Core/Shell Nanoparticles and Direct Spectroscopic Identification of Dopant Sites at the Surface and in the Interior of the Particles. *J. Am. Chem. Soc.* **2004**, *126*, 14935−14942.
(15) Binnemans, K. Interpretation of Europium(III) Spectra. *Coord. Chem. Rev.* **2015**, *295*, 1−45.
(16) Haase, M.; Riwotzki, K.; Meyssamy, H.; Kornowski, A. Synthesis and Properties of Colloidal Lanthanide-doped Nanocrystals. *J. Alloys Compd.* **2000**, *303*−*304*, 191−197.
(17) Yu, L.; Song, H.; Lu, S.; Liu, Z.; Yang, L.; Kong, X. Luminescent Properties of LaPO4: Eu Nanoparticles and Nanowires. *J. Phys. Chem. B* **2004**, *108*, 16697−16702.
(18) Ruan, Y.; Xiao, Q.; Luo, W.; Li, R.; Chen, X. Optical Properties and Luminescence Dynamics of Eu3+ Doped Terbium Orthophosphate Nanophosphors. *Nanotechnology* **2011**, *22*, 275701.
(19) Senden, T.; Rabouw, F. T.; Meijerink, A. Photonic Effects on the Radiative Decay Rate and Luminescence Quantum Yield of Doped Nanocrystals. *ACS Nano* **2015**, *9*, 1801−1808.
(20) Koole, R.; van Schooneveld, M.; Hilhorst, J.; de Mello Donega, C.; Hart, D. C.; van Blaaderen, A.; Vanmaekelbergh, D.; Meijerink, A. On the Incorporation Mechanism of Hydrophobic Quantum Dots in Silica Spheres by a Reverse Microemulsion Method. *Chem. Mater.* **2008**, *20*, 2503−2512.
(21) van Hest, J. J. H. A.; Blab, G. A.; Gerritsen, H. C.; de Mello Donega, C.; Meijerink, A. Incorporation of Ln-doped LaPO4 Nanocrystals as Luminescent Markers in Silica Nanoparticles. *Nanoscale Res. Lett.* **2016**, *11*, 261.
(22) Scherrer, P. Bestimmung der Inneren Struktur und der Größe von Kolloidteilchen mittels Röntgenstrahlen. *Göttinger Nachrichten Math. Phys.* **1918**, *2*, 98−100.
(23) Holzwarth, U.; Gibson, N. The Scherrer Equation versus the 'Debye-Scherrer Equation'. *Nat. Nanotechnol.* **2011**, *6*, 534.
(24) Martínez, J. R.; Palomares-Sánchez, S.; Ortega-Zarzosa, G.; Ruiz, F.; Chumakov, Y. Rietveld Refinement of Amorphous SiO_2 Prepared via Sol-Gel Method. *Mater. Lett.* **2006**, *60*, 3526−3529.
(25) Henderson, B.; Imbusch, G. F. *Optical Spectroscopy of Inorganic Solids*; Oxford Science Publications: Oxford, 1989.
(26) Görller-Walrand, C.; Binnemans, K.; Gschneidner, K. A. L., Jr. *Handbook on the Physics and Chemistry of Rare Earths*; Elsevier: Amsterdam, 1996; Vol. *23*.
(27) Tanner, P. Some Misconceptions Concerning the Electronic Spectra of Tri-Positive Europium and Cerium. *Chem. Soc. Rev.* **2013**, *42*, 5090−5101.
(28) Boyer, J. C.; Vetrone, F.; Capobianco, J. A.; Speghini, A.; Bettinelli, M. Variation of Fluorescence Lifetimes and Judd-Ofelt Parameters Between Eu^{3+} doped Bulk and Nanocrystalline Cubic Lu_2O_3. *J. Phys. Chem. B* **2004**, *108*, 20137−20143.
(29) Weber, M. J. *Handbook of Optical Materials*; CRC Press: Boca Raton, FL, 2003.
(30) Blasse, G.; Bril, A.; Nieuwpoort, W. C. On the Eu^{3+} Fluorescence in Mixed Metal Oxides. *J. Phys. Chem. Solids* **1966**, *27*, 1587−1592.
(31) Jørgensen, C. K.; Judd, B. R. Hypersensitive Pseudoquadrupole Transitions in Lanthanides. *Mol. Phys.* **1964**, *8*, 281−290.
(32) Werts, M. H. V.; Jukes, R. T. F.; Verhoeven, J. W. The Emission Spectrum and the Radiative Lifetime of Eu^{3+} in Luminescent Lanthanide Complexes. *Phys. Chem. Chem. Phys.* **2002**, *4*, 1542−1548.
(33) van Dijk, J. M. F.; Schuurmans, M. F. H. On the Non-Radiative and Radiative Decay Rates and a Modified Exponential Energy Gap Law for 4f-4f Transitions in Rare-Earth Ions. *J. Chem. Phys.* **1983**, *78*, 5317−5323.
(34) Chen, D.; Huang, P. Highly Intense Upconversion Luminescence in Yb/Er:$NaGdF_4$@$NaYF_4$ Core-Shell Nanocrystals with Complete Shell Enclosure of the Core. *Dalton Trans.* **2014**, *43*, 11299−11304.
(35) Stouwdam, J. W.; Hebbink, G. A.; Huskens, J.; van Veggel, F. C. J. M. Lanthanide-doped Nanoparticles with Excellent Luminescent Properties in Organic Media. *Chem. Mater.* **2003**, *15*, 4604−4616.
(36) Scorciapino, M.; Sanna, R.; Ardu, A.; Orru, F.; Casu, M.; Musinu, A.; Cannas, C. Core-Shell Nano-architectures: The Incorporation Mechanism of Hydrophobic Nanoparticles Into the Aqueous Core of a Microemulsion. *J. Colloid Interface Sci.* **2013**, *407*, 67−75.

DOI: 10.1021/acs.jpcc.7b06549
J. Phys. Chem. C 2017, 121, 19373−19382